JOURNAL OF GUIDANCE, CONTROL, AND DYNAMICS
Vol. 32, No. 1, January–February 2009

Engineering Notes

ENGINEERING NOTES are short manuscripts describing new developments or important results of a preliminary nature. These Notes should not exceed 2500 words (where a figure or table counts as 200 words). Following informal review by the Editors, they may be published within a few months of the date of receipt. Style requirements are the same as for regular contributions (see inside back cover).

Robust Aeroelastic Control of Lifting Surfaces with Uncertainty via Multi-Objective Synthesis

Sungsoo Na,* In-Joo Jeong,† and Gwon-Chan Yoon‡
Korea University, Seoul 136-701, Republic of Korea
and
Pier Marzocca§
Clarkson University, Potsdam, New York 13699

DOI: 10.2514/1.36071

I. Introduction

A GREAT deal of research activity devoted to the aeroelastic active control and flutter suppression of flight vehicles has been accomplished so far [1]. A number of recent contributions related to the active control of an aircraft wing are discussed at length in [2–4]. Digital adaptive control of a linear aeroservoelastic model [5], the μ method for robust aeroservoelastic stability analysis [6], gain scheduled controllers [7], and neural and adaptive control of a transonic wind-tunnel model [8,9] are only a few of the latest active control methods that have been developed. Linear control theory, the feedback linearizing technique, and adaptive control strategies have been derived to account for the effect of nonlinear structural stiffness [10]. A model reference variable structure adaptive control system for plunge displacement and pitch angle control has been designed using bounds on uncertain functions [11]. This approach yields a high gain feedback discontinuous control system. In [12–14], an adaptive design method for flutter suppression has been adopted while using measurements of either and both the pitching and plunging variables. To supplement the bulk of knowledge of the robust aeroelastic control of lifting surfaces present in the literature, in this paper a linear matrix inequality (LMI) approach for the multi-objective synthesis is considered. A multi-objective state-feedback control law implementing mixed control strategy with a pole placement constraint will be implemented and some of its performance characteristics will be highlighted. The design objective to be achieved is a mix of H_∞ performance and H_2 performance satisfying constraints on the closed-loop pole locations in the presence of model uncertainties. The traditional 3-DOF aeroelastic model for the control of a thin airfoil in incompressible flow is used for such purpose.

Received 5 December 2007; accepted for publication 16 September 2008.

*Professor, 1ga, Anam-dong, Seongbuk-gu.
†Graduate Student, 1ga, Anam-dong, Seongbuk-gu.
‡Graduate Student, 1ga, Anam-dong, Seongbuk-gu.
§Assistant Professor, Mechanical and Aeronautical Engineering Department, 8 Clarkson Avenue.

II. Configuration of the Aeroelastic Model

Figure 1 presents the typical flapped wing system used in the present aeroelastic analysis. The 3-degree-of-freedom lifting surface of chord length $2b$ is modeled by the plunge h (positive downward), pitch angle α (measured from the horizontal at the elastic axis, positive clockwise), and the control flap angle β (positive flap down) displacements. Consequently, this is a six-dimensional linear aeroelastic system with the following states: plunging displacement, pitching angle, flap angle, and their rates. The pitching and plunging displacements are restrained by a pair of linear springs attached to the elastic axis (EA) with spring constants K_α and K_h, respectively, whereas the control flap torsional spring of constant K_β is located at the flap hinge. The reference axes x and z are located at the elastic axis; the EA is located at distance db from the leading edge and at distance x_{EA} from middle-chord point, whereas the flap hinge is located at distance rb from the elastic axis.

The wing is situated in a fluid with a freestream velocity, V. The lift L (positive upward in the positive z direction), the aerodynamic pitching moment M (measured counterclockwise and evaluated at the quarter-chord), and the torque T (measured counterclockwise and applied at the flap hinge) can be seen as three inputs applied to the aeroelastic system. The torque applied at the flap consists of the torque generated by the air flow and the external torque that can be applied by an actuator.

The fluid is assumed to be incompressible and irrotational. Because of these assumptions, the result is an irrational and improper transfer matrix from the degrees of freedom to the lift, aerodynamic moment, and hinge torque [15]; taking a standard second-order rational approximation to the Theodorsen function, it is possible to get an improper rational transfer matrix that can be connected in feedback with the proper transfer matrix from lift, moment, and hinge torque to plunge, pitch angle, and flap angle. The complete model is a proper linear system that can be realized by a ten-dimensional state-space model. The one-dimensional control is the additional torque that is applied at the hinge by the actuator.

III. Governing Equations of the Aeroelastic Model

The aeroelastic model is usually the interconnection of two submodels describing 1) how the aerodynamic forces affect the motion of the wing section, and 2) how the motion of the wing section affects the aerodynamic forces. The first submodel is a state-space model derived from classical mechanics, whereas the second submodel is usually realized in the frequency domain by solving an unsteady Laplace partial differential equation and then it is approximated by a state-space model. In matrix form, the aeroelastic governing equations of the 3-DOF airfoil can be written as follows [1]:

$$\mathbf{M}\ddot{\mathbf{y}}(t) + \mathbf{K}\mathbf{y}(t) = -\mathbf{L}(t) + \mathbf{L}_b(t) + \mathbf{L}_c(t) \tag{1}$$

where $\mathbf{L}(t)$, $\mathbf{L}_b(t)$, and $\mathbf{L}_c(t)$ represent the unsteady aerodynamic, blast, and control loads, respectively. In Eq. (1), the column vector of plunging, pitching, and flapping displacements is defined as

$$\mathbf{y}(t) = \left\{ (h(t)/b) \quad \alpha(t) \quad \beta(t) \right\}^T \tag{2}$$

while

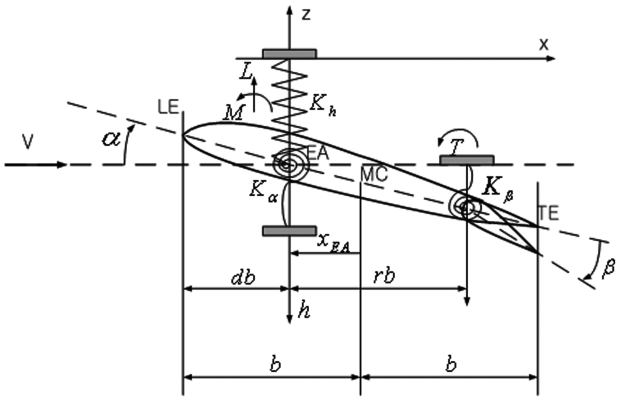

Fig. 1 Typical 3-DOF plunging–pitching–flapping lifting surface.

$$\mathbf{M} = \begin{bmatrix} bm & S_\alpha & S_\beta \\ bS_\alpha & I_\alpha & I_\beta + bcS_\beta \\ bS_\beta & I_\beta + bcS_\beta & I_\beta \end{bmatrix} \tag{3}$$

$$\mathbf{K} = \begin{bmatrix} bK_h & 0 & 0 \\ 0 & K_\alpha & 0 \\ 0 & 0 & K_\beta \end{bmatrix} \tag{4}$$

denote the mass and stiffness matrices, respectively. By combining Eqs. (1–4), the second-order aeroelastic governing equation can be cast in a family of linear first-order state-space models parametrized by the freestream airspeed V of the form

$$\dot{\mathbf{x}}(t) = \mathbf{A}\mathbf{x}(t) + \mathbf{B}u(t) + \mathbf{G}w(t) \tag{5}$$

Here A is the aerodynamic matrix [15]. The eigenvalues of A change with the freestream velocity V. At low velocities, all the eigenvalues are in the open left-half plane. But as the speed increases, the system loses stability as a pair of eigenvalues moves across the imaginary axis to the right-half plane. The ten-dimensional state vector is given by

$$\mathbf{x}(t) = \{\, \dot{h}(t)/b \quad \dot{\alpha}(t) \quad \dot{\beta}(t) \quad h(t)/b \quad \alpha(t) \quad \beta(t) \quad B_1(t) \quad B_2(t) \quad A_1(t) \quad A_2(t) \,\}^T \tag{6}$$

where $B_1(t)$, $B_2(t)$, $A_1(t)$, and $A_2(t)$ denote aerodynamic lag states; $u(t)$ is control input; $w(t)$ is an external disturbance represented by a time-dependent external excitation; and $\mathbf{G}$ is the disturbance-input matrix, whereas $\mathbf{B}$ is the control input matrix that is given by

$$\mathbf{B} = (1/I_\beta)\{\{\mathbf{M}^{-1}\{0 \quad 0 \quad 1\}^T\}^T \quad 0 \quad 0 \quad 0 \quad 0 \quad 0 \quad 0 \quad 0\}^T \tag{7}$$

The aerodynamic load vector appearing in Eq. (1) is expressed in terms of its components as

$$\mathbf{L}(t) = \{\, L_T(t) \quad M_T(t) \quad T_T(t) \,\}^T \tag{8}$$

where $L_T(t)$, $M_T(t)$, and $T_T(t)$ denote the lift, the aerodynamic moment, and the flap, respectively [15]:

$$L_T(t) = \pi\rho b^2[\ddot{h}(t) - bx_{\mathrm{EA}}\ddot{\alpha}(t) + (b/2\pi)\Phi_4\ddot{\beta}(t) + V_f\dot{\alpha}(t) + (V_f/\pi)\Phi_3\dot{\beta}(t)] + 2\pi\rho V_f bD(t) \tag{9a}$$

$$M_T(t) = \pi\rho b^3\Big[-x_{\mathrm{EA}}\ddot{h}(t) + b\Big(\tfrac{1}{8} + x_{\mathrm{EA}}^2\Big)\ddot{\alpha}(t) + (b/4\pi)\Phi_7\ddot{\beta}(t) + (\tfrac{1}{2} - x_{\mathrm{EA}})V_f\dot{\alpha} + (V_f/2\pi)\Phi_6\dot{\beta}(t) + \Big(V_f^2/\pi b\Big)\Phi_5\beta(t)\Big] - 2\pi\rho b^2(\tfrac{1}{2} + x_{\mathrm{EA}})V_f D(t) \tag{9b}$$

$$T_T(t) = \pi\rho b^2\Big[\Big(\frac{b}{2\pi}\Phi_4\Big)\ddot{h}(t) + \Big(\frac{b^2}{4\pi}\Phi_7\Big)\ddot{\alpha}(t) + \Big(\frac{b^2}{2\pi^2}\Phi_{12}\Big)\ddot{\beta}(t) + \Big(\frac{bV_f}{2\pi}\Phi_9\Big)\dot{\alpha} + \Big(\frac{bV_f}{2\pi^2}\Phi_{11}\Big)\dot{\beta}(t) + \Big(\frac{V_f^2}{\pi^2}\Phi_{10}\Big)\beta(t)\Big] + \pi\rho V_f bP(t) \tag{9c}$$

Herein Φ_i are the Theodorsen constants. See [15] for details about the aerodynamic representation.

IV. Multi-Objective State-Feedback Control Methodology

In the present work, it is assumed that all six physical states are measurable and available. The dynamic state feedback based on the linear matrix inequality scheme for the multi-objective synthesis is then implemented. The stability and robustness of the six states are explored and compared with suboptimal H controllers. One major difficulty with these approaches is that they must be scheduled on a parameter, the freestream airspeed. The usual approach is to choose several parameter values, that is, freestream speeds, and design a controller at each one by solving one or more algebraic Riccati equations. Near a parameter value, one uses the appropriate controller, but between parameter values, one must interpolate between controller values in some fashion, for example, piecewise linear interpolation. In many control problems, the design specifications are based on a mix of performance and robustness objectives expressed both in the time and frequency domains. These various objectives are rarely satisfied with a single synthesis. In this sense, through multi-objective control, a number of control objectives can be obtained [16,17]. Multi-objective robust design pertains to the so-called mixed H_∞/H_2 problem, and it corresponds to the robust stability and nominal performance for state-feedback and output-feedback cases [18]. In this paper, a multi-objective state-feedback control methodology is implemented for the control of a wing section. Such a control methodology satisfies the following three objectives:

1) The H_∞ performance is convenient to enforce robustness to model uncertainty and to express frequency domain specifications. Herein, a suboptimal controller is considered. The H_∞ control problem is to find all admissible controllers $K(s)$, if there are any, such that the H_∞ norm of the transfer matrix $\mathbf{T}_{\mathbf{wz}_\infty}$ from $\mathbf{w}$ to $\mathbf{z}_\infty$ is less than a given disturbance attenuation, γ, that is, $\|\mathbf{T}_{\mathbf{wz}_\infty}\|_\infty < \boldsymbol{\gamma}$. $\mathbf{T}_{\mathbf{wz}_\infty}(s)$ denotes the closed-loop transfer function from $\mathbf{w}(t)$ to $\mathbf{z}_\infty(t)$.

2) The H_2 performance is useful for handling stochastic aspects such as measurement noise and random disturbance. The H_2 control problem is to find a proper real rational controller $K(s)$ that stabilizes $T_{wz_2}(s)$ internally and minimizes the H_2 norm of the transfer matrix $\mathbf{T}_{\mathbf{wz}_2}$ from $\mathbf{w}$ to $\mathbf{z}_2$; for example, $\|\mathbf{T}_{\mathbf{wz}_2}\|_2 \cdot \mathbf{T}_{\mathbf{wz}_2}(s)$ denotes the closed-loop transfer function from $\mathbf{w}(t)$ to $\mathbf{z}_2(t)$, respectively

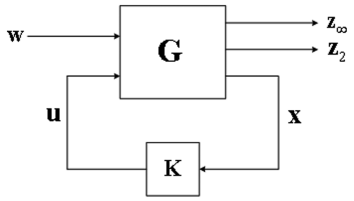

Fig. 2 Standard H_∞/H_2 state-feedback structure.

3) The regional pole placement constraints guarantee the desirable minimum decay rate of closed-loop damping. In addition, the pole placement constraints ensure fast and well-damped transient responses and a reasonable feedback gain.

In summary, the multi-objective design allows for a more flexible and accurate specification of the desirable closed-loop behavior. The basic configuration of the multi-objective state-feedback control system is shown in Fig. 2. A linear time invariant system is described by the state equations as follows:

$$\begin{aligned}\dot{\mathbf{x}}(t) &= \mathbf{A}\mathbf{x}(t) + \mathbf{B}_1\mathbf{w}(t) + \mathbf{B_2}\mathbf{u}(t)\\ \mathbf{z}_\infty(t) &= \mathbf{C_1}\mathbf{x}(t) + \mathbf{D_{11}}\mathbf{w}(t) + \mathbf{D_{12}}\mathbf{u}(t)\\ \mathbf{z_2}(t) &= \mathbf{C_2}\mathbf{x}(t) + \mathbf{D_{21}}\mathbf{w}(t) + \mathbf{D_{22}}\mathbf{u}(t)\\ \mathbf{y}(t) &= \mathbf{C_y}\mathbf{x}(t) + \mathbf{D_{y1}}\mathbf{w}(t) + \mathbf{D_{y2}}\mathbf{u}(t)\end{aligned} \tag{10}$$

where $\mathbf{x}(t)$: $\mathbb{R}_+ \to \mathbb{R}^n$, $\mathbf{u}(t)$: $\mathbb{R}_+ \to \mathbb{R}^{n_u}$, $\mathbf{w}(t)$: $\mathbb{R}_+ \to \mathbb{R}^{n_w}$, $\mathbf{z}_\infty(t)$: $\mathbb{R}_+ \to \mathbb{R}^{n_{z\infty}}$, $\mathbf{z}_2(t)$: $\mathbb{R}_+ \to \mathbb{R}^{n_{z2}}$, and $\mathbf{y}(t)$: $\mathbb{R}_+ \to \mathbb{R}^{n_y}$; $\mathbf{x}(t)$ is the state, $\mathbf{u}(t)$ is the control input, $\mathbf{w}(t)$ is the exogenous input, and $\mathbf{z}_\infty(t)$ and $\mathbf{z}_2(t)$ are the regulated output, whereas $\mathbf{y}(t)$ is the measured output. It is also assumed that the states can be measured or estimated and a constant state-feedback controller of the form $\mathbf{u} = \mathbf{K}_C\mathbf{x}$ is used. In other words, $\mathbf{C_y} = \mathbf{I}, \mathbf{D_{y2}} = \mathbf{D_{y1}} = \mathbf{0}$. Therefore, the closed-loop system is given in state-space form as

$$\begin{aligned}\dot{\mathbf{x}}(t) &= (\mathbf{A} + \mathbf{B_2}\mathbf{K}_C)\mathbf{x}(t) + \mathbf{B}_1\mathbf{w}(t)\\ \mathbf{z}_\infty(t) &= (\mathbf{C_1} + \mathbf{D_{12}}\mathbf{K}_C)\mathbf{x}(t) + \mathbf{D_{11}}\mathbf{w}(t)\\ \mathbf{z_2}(t) &= (\mathbf{C_2} + \mathbf{D_{22}}\mathbf{K}_C)\mathbf{x}(t) + \mathbf{D_{21}}\mathbf{w}(t)\end{aligned} \tag{11}$$

A. H_∞ Performance

A linear system described by the state equations [19] is considered:

$$\begin{aligned}\dot{\mathbf{x}}(t) &= \mathbf{A}\mathbf{x}(t) + \mathbf{B}_1\mathbf{w}(t) + \mathbf{B_2}\mathbf{u}(t)\\ \mathbf{z}_\infty(t) &= \mathbf{C_1}\mathbf{x}(t) + \mathbf{D_{11}}\mathbf{w}(t) + \mathbf{D_{12}}\mathbf{u}(t)\\ \mathbf{y}(t) &= \mathbf{C_y}\mathbf{x}(t) + \mathbf{D_{y1}}\mathbf{w}(t) + \mathbf{D_{y2}}\mathbf{u}(t)\end{aligned} \tag{12}$$

The basic configuration of the feedback system is shown in Fig. 3. Also, in this case it is assumed that the full state can be measured or estimated. By assuming $\mathbf{C_y} = \mathbf{I}, \mathbf{D_{y1}} = \mathbf{D_{y2}} = \mathbf{0}$, and $\mathbf{u} = \mathbf{K}_C\mathbf{x}$, the closed-loop state equations [16] can be obtained. These are

$$\begin{aligned}\dot{\mathbf{x}}(t) &= (\mathbf{A} + \mathbf{B_2}\mathbf{K}_C)\mathbf{x}(t) + \mathbf{B}_1\mathbf{w}(t)\\ \mathbf{z}_\infty(t) &= (\mathbf{C_1} + \mathbf{D_{12}}\mathbf{K}_C)\mathbf{x}(t) + \mathbf{D_{11}}\mathbf{w}(t)\end{aligned} \tag{13}$$

The standard H_∞ performance of control looks at minimizing the H_∞ norm of the transfer function $\mathbf{w}(t)$ to $\mathbf{z}_\infty(t)$. The H_∞-norm concept in optimal control theory is defined in the frequency domain for a stable transfer function $\mathbf{T}(s)$ as

$$\|\mathbf{T}\|_\infty := \sup_\omega \sigma_{\max}[\mathbf{T}(j\omega)] \qquad (\sigma_{\max} := \text{maximum singular value}) \tag{14}$$

The constraint $\|\mathbf{T}_{\mathbf{wz}_\infty}\|_\infty < \boldsymbol{\gamma}$ can be interpreted as a disturbance rejection performance and robust stability of the closed-loop system. By using the H_∞ control with a given constant $\gamma > 0$, the system equation (13) could be stabilized with disturbance attenuation γ if there exists a state-feedback matrix $\mathbf{K}_C \in \mathbb{R}^{n_u \times n}$ such that the following conditions are satisfied: 1) the matrix $\mathbf{A}_{\text{cl}} = \mathbf{A} + \mathbf{B}_2\mathbf{K}_C$ is a stability matrix, that is, all the eigenvalues of $\mathbf{A}_{\text{cl}}$ lie in the open left-half plane; and 2) the closed-loop transfer function matrix

$$\|\mathbf{T}_{\mathbf{wz}_\infty}\|_\infty < \boldsymbol{\gamma} \tag{15}$$

for all $\omega \in \mathbb{R}$. This implies that the H_∞ norm of $\mathbf{T}_{\mathbf{wz}_\infty}(s) = (\mathbf{C_1} + \mathbf{D_{11}}\mathbf{K}_C)(s\mathbf{I} - \mathbf{A} - \mathbf{B_2}\mathbf{K}_C)^{-1}\mathbf{B_1} + \mathbf{D_{21}}$ is less than γ. The influence of disturbance $\mathbf{w}$ on the output $\mathbf{z}_\infty$ is measured by the H_∞ norm of the transfer matrix $\mathbf{T}_{\mathbf{wz}_\infty}(s)$. By applying the bounded-real lemma and Shur complement [17] to the closed-loop system, the H_∞ performance LMI) conditions can be obtained:

$$\begin{bmatrix} \mathbf{A}\mathbf{Q}_\infty + \mathbf{Q}_\infty\mathbf{A}^T + \mathbf{B_2}\mathbf{L} + \mathbf{L}^T\mathbf{B_2}^T & \mathbf{B_1} & \mathbf{Q}_\infty\mathbf{C}_\infty^T + \mathbf{L}^T\mathbf{D}_{12}^T \\ \mathbf{B}_1^T & -\gamma^2\mathbf{I} & \mathbf{D}_{11}^T \\ \mathbf{C_1}\mathbf{Q}_\infty + \mathbf{D_{12}}\mathbf{L} & \mathbf{D_{11}} & -\mathbf{I} \end{bmatrix} \le 0, \qquad \mathbf{Q}_\infty > 0 \tag{16}$$

where the function $\mathbf{L} = \mathbf{K}_C\mathbf{Q}$ has been introduced. The problem is converted to a convex optimization problem, linear in $\mathbf{Q}$ and $\mathbf{L}$. The optimal solution is computed by minimizing γ over the variables $\mathbf{Q}$, $\mathbf{L}$, and γ to satisfy the conditions in Eqs. (16). If Eqs. (16) are satisfied, $(\mathbf{Q}^*, \mathbf{L}^*, \gamma^*)$ represent an optimal solution of this eigenvalue problem, such that the state-feedback control gain $\mathbf{K}_C = \mathbf{L}(\mathbf{Q}^*)^{-1}$ has guaranteed H_∞ performance that is less than γ^*.

B. H_2 Performance

A standard feedback control system for the H_2 control problem is represented as [16]

$$\begin{aligned}\dot{\mathbf{x}}(t) &= \mathbf{A}\mathbf{x}(t) + \mathbf{B}_1\mathbf{w}(t) + \mathbf{B_2}\mathbf{u}(t)\\ \mathbf{z_2}(t) &= \mathbf{C_2}\mathbf{x}(t) + \mathbf{D}_{21}\mathbf{w}(t) + \mathbf{D_{22}}\mathbf{u}(t)\\ \mathbf{y}(t) &= \mathbf{C_y}\mathbf{x}(t) + \mathbf{D_{y1}}\mathbf{w}(t) + \mathbf{D_{y2}}\mathbf{u}(t)\end{aligned} \tag{17}$$

Also, in this case it is assumed that $\mathbf{C_y} = \mathbf{I}, \mathbf{D}_{21} = \mathbf{D_{y1}} = \mathbf{D_{y2}} = \mathbf{0}$. The standard configuration of the H_2 feedback system is shown in Fig. 4.

Using a feedback controller such as $\mathbf{u}(t) = \mathbf{K}_C\mathbf{x}(t)$ or $\mathbf{u}(t) = \mathbf{K}_C\mathbf{y}(t)$, a short-hand notation of the closed-loop system can be introduced such that

$$\dot{\mathbf{x}}(t) = \mathbf{A_{cl}}\mathbf{x}(t) + \mathbf{B}_1\mathbf{w}(t), \qquad \mathbf{z}_2(t) = \mathbf{C_{cl}}\mathbf{x}(t) \tag{18}$$

where $\mathbf{A}_{\text{cl}} = \mathbf{A} + \mathbf{B_2}\mathbf{K}_C$, $\mathbf{C}_{\text{cl}} = \mathbf{C_2} + \mathbf{D_{22}}\mathbf{K}_C$, and $\|\mathbf{T}_{\mathbf{wz}_2}\|_2^2 = \text{trace}(\mathbf{C_{cl}}\mathbf{Q_c}\mathbf{C_{cl}^T})$; see, for example, [18]. $\mathbf{Q_c}$ is the solution of the Lyapunov equation and controllability gramian, such that

$$\mathbf{A}_{\mathbf{cl}}\mathbf{Q_c} + \mathbf{Q_c}\mathbf{A}_{\mathbf{cl}}^T + \mathbf{B_1}\mathbf{B_1}^T = \mathbf{0} \tag{19}$$

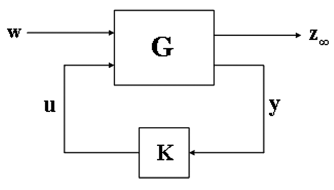

Fig. 3 Standard H_∞ feedback structure.

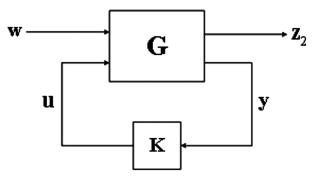

Fig. 4 Standard H_2 feedback structure.

Hence $\|\mathbf{T}_{wz_2}\|_2^2 = \text{trace}(\mathbf{C_{cl}Q_cC_{cl}^T})$ for any symmetric $\mathbf{Q_2} > \mathbf{Q_c} > 0$, such that

$$\mathbf{A}_{\mathbf{cl}}\mathbf{Q_2} + \mathbf{Q_2}\mathbf{A}_{\mathbf{cl}}^T + \mathbf{B_1}\mathbf{B_1} < \mathbf{0} \tag{20}$$

Equivalently, it is possible to write $\|\mathbf{T}_{wz_2}\|_2^2 = \text{trace}(\mathbf{C_{cl}Q_cC_{cl}^T}) < \text{trace}(\mathbf{C_{cl}Q_2C_{cl}^T})^{\mathbf{T}} < \text{trace}(\mathbf{Y})$ whenever the symmetric matrices $\mathbf{Q_2}$ and $\mathbf{Y}$ satisfy the following inequalities:

$$\begin{bmatrix} (\mathbf{A}+\mathbf{B_2K}_C)\mathbf{Q}+\mathbf{Q}(\mathbf{A}+\mathbf{B_2K}_C)^T & \mathbf{B_1} \\ \mathbf{B_1}^T & -\mathbf{I} \end{bmatrix} < \mathbf{0}$$
$$\begin{bmatrix} \mathbf{Y} & (\mathbf{C_2}+\mathbf{D_{22}K}_C)\mathbf{Q} \\ \mathbf{Q}(\mathbf{C_2}+\mathbf{D_{22}K}_C)^T & \mathbf{Q} \end{bmatrix} > \mathbf{0}, \qquad \mathbf{Q} > \mathbf{0} \tag{21}$$

By introducing $\mathbf{L} = \mathbf{K}_C\mathbf{Q_2}$, these LMI conditions are converted to a convex optimization problem [19], which means that Eq. (21) is expressed as

$$\begin{bmatrix} \mathbf{AQ_2}+\mathbf{Q_2A}^T+\mathbf{B_2L}+\mathbf{L}^T\mathbf{B_2}^T & \mathbf{B_1} \\ \mathbf{B_1}^T & -\mathbf{I} \end{bmatrix} < 0$$
$$\begin{bmatrix} \mathbf{Y} & \mathbf{C_2Q_2}+\mathbf{D_{22}L} \\ \mathbf{Q_2C_2}^T+\mathbf{L}^T\mathbf{D_{22}}^T & \mathbf{Q_2} \end{bmatrix} > 0 \tag{22}$$

We can compute the solution of the state problem by minimizing $\mathbf{Y}$, satisfying the conditions (22). If Eqs. (22) are realizable, $(\mathbf{Y}^*, \mathbf{Q}^*, \mathbf{L}^*)$ represent an optimal solution of this problem. Then state-feedback control gain $\mathbf{K}_C^* = \mathbf{L}(\mathbf{Q}^*)^{-1}$ has guaranteed $\|\mathbf{T}_{wz_2}\|_2 < \sqrt{\text{trace}(\mathbf{Y}^*)}$.

C. Regional Pole Constraints

It is known that the transient response of a linear system is related to the locations of its poles [20]. Pole assignment in convex regions of the left-half plane can also expressed as LMI constraints on the Lyapunov matrix $\mathbf{Q}$. Regions of interest include α-stability regions $Re \leq -\alpha$, vertical strips, disks, conic sectors, etc. Another interesting region for control purposes is the set $S(\alpha, r, \theta)$ of complex numbers $x + jy$ such that

$$x < -\alpha < 0 \tag{23a}$$

$$|x + jy| < r \tag{23b}$$

$$\tan(\theta/2)x < -|y| \tag{23c}$$

Confining the closed-loop poles to this region ensures a minimum decay rate α, a minimum damping ratio $\zeta = \cos(\theta/2)$, and a maximum damped natural frequency $\omega_d = r\sin(\theta/2)$. Consequently, this bounds the maximum overshoot, the frequency of oscillatory modes, the delay time, the rise time, and the settling time.

LMI regions include relevant sections, such as sectors, disks, conics, strips, etc., as well as any of their intersections. The standard Lyapunov theorem for the open left-half plane with characteristic function $f_R = \{z \in \mathbb{C}: z + \bar{z} < 0\}$ can be generalized to the following arbitrary LMI regions:

1) The disk is centered at $(-q, 0)$ and radius r, such that

$$f_R(z) = \begin{bmatrix} -r & \bar{z}+q \\ z+q & -r \end{bmatrix} \tag{24}$$

2) The conic sector is centered at the origin and with inner angle θ, such that

$$f_R(z) = \begin{bmatrix} \sin\frac{\theta}{2}(z+\bar{z}) & -\cos\frac{\theta}{2}(z-\bar{z}) \\ \cos\frac{\theta}{2}(z-\bar{z}) & \sin\frac{\theta}{2}(z+\bar{z}) \end{bmatrix} \tag{25}$$

This ensures that the damping ratio of poles lying in this sector is at least equal to $\cos(\theta/2)$.

3) The vertical strips are located at h_1 and h_2, such that

$$f_R(z) = \begin{bmatrix} 2h_1-(z+\bar{z}) & 0 \\ 0 & (z+\bar{z})-2h_2 \end{bmatrix} \tag{26}$$

A subset $\Re$ of the complex plane is called the LMI region if there exist a symmetric matrix $\alpha = [\alpha_{kl}] \in \mathbb{R}^{m\times m}$ and matrix $\beta = [\beta_{kl}] \in \mathbb{R}^{m\times m}$ such that

$$\Re = \{z \in \mathbb{C}: f_R(z) < 0\} \tag{27}$$

with

$$f_R(z) = \alpha + z\beta + \bar{z}\beta^T = [\alpha_{kl} + \beta_{kl}z + \beta_{lk}\bar{z}]_{1\leq k,l\leq m} \tag{28}$$

Specifically, the pole location in a given LMI region can be characterized in terms of the $m \times m$ block matrix

$$M_{\Re}(\mathbf{A}, \mathbf{Q}) := \alpha \otimes \mathbf{Q} + \beta \otimes (\mathbf{AQ}) + \beta^T \otimes (\mathbf{AQ})^T$$
$$= [\alpha_{kl}\mathbf{Q} + \beta_{kl}\mathbf{AQ} + \beta_{lk}\mathbf{QA}^T]_{1\leq k,l\leq m} \tag{29}$$

The matrix $\mathbf{A}$ is $\Re$ stable if and only if there exists a symmetric matrix $\mathbf{Q}$ such that [20]

$$M_{\Re}(\mathbf{A}, \mathbf{Q}) < 0, \qquad \mathbf{Q} > 0 \tag{30}$$

Equation (30) enables us to transform Eqs. (24–26) into the following LMI formulations of prescribed pole clustering regions.

4) The disk of radius r and center $(-q, 0)$ is an LMI region with characteristic function Eq. (24)

$$\begin{bmatrix} -r\mathbf{Q} & q\mathbf{Q}+\mathbf{QA}^T \\ q\mathbf{Q}+\mathbf{AQ} & -r\mathbf{Q} \end{bmatrix} < 0, \qquad \mathbf{Q} > 0 \tag{31}$$

5) The conic sector centered at the origin with inner angle θ and with characteristic function Eq. (25) yields

$$\begin{bmatrix} \sin\frac{\theta}{2}(\mathbf{AQ}+\mathbf{QA}^T) & -\cos\frac{\theta}{2}(\mathbf{AQ}-\mathbf{QA}^T) \\ \cos\frac{\theta}{2}(\mathbf{AQ}-\mathbf{QA}^T) & \sin\frac{\theta}{2}(\mathbf{AQ}+\mathbf{QA}^T) \end{bmatrix} < 0, \qquad \mathbf{Q} > 0 \tag{32}$$

6) The vertical strip with characteristic function Eq. (26) is

$$\begin{bmatrix} 2h_1-(\mathbf{AQ}+\mathbf{QA}^T) & 0 \\ 0 & (\mathbf{AQ}+\mathbf{QA}^T)-2h_2 \end{bmatrix} < 0, \qquad \mathbf{Q} > 0 \tag{33}$$

It can be summarized for the closed-loop system [20] in the following manner

$$M_{\Re}(\mathbf{A_{cl}}, \mathbf{Q}_{\Re}) < 0, \qquad \mathbf{Q}_{\Re} > 0 \tag{34}$$

In the previews equations, several time and frequency domain specifications have been expressed as LMI constraints on the closed-loop state-space matrices. These specifications are now used for multi-objective synthesis purposes. For a prescribed closed-loop H_∞ performance $\gamma > 0$, the suboptimal mixed H_∞/H_2 problem consists of finding a state-feedback gain $\mathbf{K}_C$ that 7) places the closed-loop poles in some LMI stability region $\Re$, 8) guarantees the H_∞ performance $\|\mathbf{T}_{wz_\infty}\|_\infty < \boldsymbol{\gamma}$, and 9) minimizes the H_2 performance $\|\mathbf{T}_{wz_2}\|_2$ subjected to the two previous constraints.

The goal of such approach is to minimize the H_2 norm of $\|\mathbf{T}_{wz_2}\|_2$ over all state-feedback gains that enforce H_∞ and pole constraints. From the earlier discussion, this is equivalent to minimizing the trace$(\mathbf{Y})$ over all matrices $\mathbf{Q}_\infty$, $\mathbf{Q_2}$, $\mathbf{Q}_{\Re}$, $\mathbf{Y}$, and $\mathbf{L}$ satisfying Eqs. (16), (22), and (34). To implement multi-objective synthesis, the following constraint is imposed

$$\mathbf{Q} = \mathbf{Q}_\infty = \mathbf{Q_2} = \mathbf{Q}_{\Re} \tag{35}$$

The solution can be sought by substituting Eqs. (35) into Eqs. (16), (22), and (34). The H_2 performance index is defined by

$$J(T_{wz_\infty}) :=$$
$$\inf\Big\{\text{trace}(\mathbf{Y})\text{: } \mathbf{Q}, \mathbf{Y}, \mathbf{L}, \text{satisfy Eqs.(16), (22) and (34)}$$
$$\text{with } \mathbf{Q} = \mathbf{Q}_\infty = \mathbf{Q}_2 = \mathbf{Q}_\Re\Big\} \tag{36}$$

The performance index can be computed as the global minimum of the following LMI optimization problem. In other words, minimizing the trace($\mathbf{Y}$) over $\mathbf{Q} = \mathbf{Q}^T > 0$, $\mathbf{Y} = \mathbf{Y}^T$, and $\mathbf{L}$ subject to the LMI constraints. This implies that the following four inequalities have to be verified:

$$\begin{bmatrix} \mathbf{AQ} + \mathbf{QA}^T + \mathbf{B_2L} + \mathbf{L}^T\mathbf{B}_2^T & \mathbf{B_1} & \mathbf{QC}_\infty^T + \mathbf{L}^T\mathbf{D}_{1\mathbf{u}}^T \\ \mathbf{B}_1^T & -\gamma^2\mathbf{I} & \mathbf{D}_{11}^T \\ \mathbf{C_1Q} + \mathbf{D_{12}L} & \mathbf{D_{11}} & -\mathbf{I} \end{bmatrix}$$
$$\le 0, \qquad \mathbf{Q}_\infty > 0$$
$$\begin{bmatrix} \mathbf{Y} & \mathbf{C_2Q} + \mathbf{D_{22}L} \\ \mathbf{QC}_2^T + \mathbf{LD}_{22}^T & \mathbf{Q} \end{bmatrix} > 0$$
$$\Big[\alpha_{kl}\mathbf{Q} + \beta_{kl}(\mathbf{AQ} + \mathbf{B_1L}) + \beta_{lk}\Big(\mathbf{QA}^T + \mathbf{L}^T\mathbf{B}_2^T\Big)\Big]_{1\le k,l\le m} < 0 \tag{37}$$

Also, in this case it is assumed that the system of Eqs. (37) is feasible and $(\mathbf{Q}^*, \mathbf{Y}^*, \mathbf{L}^*, \gamma^*)$ represent an optimal solution of this minimization problem. Consequently, the corresponding state-feedback control gain given by $\mathbf{K}_C^* = \mathbf{L}^*(\mathbf{Q}^*)^{-1}$ guarantees that the H_∞ performance is less than γ^*, placing the closed-loop poles in $\Re$. This also yields an H_2 performance that does not exceed $\sqrt{\text{trace}(\mathbf{Y}^*)}$. From the tradeoff curve between the H_∞ and H_2 performances, the best compromise state-feedback control gain $\mathbf{K}_C$ can be selected.

V. Model Uncertainty

The notion of an uncertain dynamical system is central to robust control theory. The gap between such models and the true physical system is called the model uncertainty. Generally, uncertainties stem from the imperfect knowledge of the system or the alteration of the physical parameter values due to changes in operation conditions. Uncertain results from physical parameters whose values are only approximately known or vary in time are also a concern. Of the various classes of uncertainty [19,3], in this paper the parameter uncertainty is considered, which originates from an imperfect knowledge of the physical parameter values or from variations of these parameters during operation. It is considered that mass and stiffness will have variations within a ±5% range of nominal value. These uncertainties are represented by uncertain state-space models. An uncertain state-space model is described as

$$\mathbf{E}\,\dot{\mathbf{x}} = \tilde{\mathbf{A}}\mathbf{x} + \tilde{\mathbf{B}}\mathbf{u}, \qquad \mathbf{y} = \mathbf{Cx} + \mathbf{Du} \tag{38}$$

where the state-space matrices $\tilde{\mathbf{A}}$, $\tilde{\mathbf{B}}$, $\mathbf{C}$, $\mathbf{D}$, and $\mathbf{E}$ depend on uncertain and/or time-varying parameters or vary in some bounded sets of the spaces of matrices. The dynamic equations of motions often involve uncertain or time-varying coefficients. When the system is linear, it naturally gives rise to parameter-dependent models of the form

$$\mathbf{E}\,(p)\dot{\mathbf{x}} = \tilde{\mathbf{A}}(p)\mathbf{x} + \tilde{\mathbf{B}}(p)\mathbf{u}, \qquad \mathbf{y} = \mathbf{C}(p)\mathbf{x} + \mathbf{D}(p)\mathbf{u} \tag{39}$$

where $\tilde{\mathbf{A}}(\cdot), \ldots, \mathbf{E}(\cdot)$ are known functions of some parameter vector $\mathbf{p} = (p_1, \ldots, p_n)$. This implies that the parameter-dependent models can be cast as

$$\begin{aligned} \tilde{\mathbf{A}}(\mathbf{p}) &= \mathbf{A}_0 + p_1\mathbf{A}_1 + \cdots + p_n\mathbf{A}_n \\ \tilde{\mathbf{B}}(\mathbf{p}) &= \mathbf{B}_0 + p_1\mathbf{B}_1 + \cdots + p_n\mathbf{B}_n \end{aligned} \tag{40}$$

and so on. $\tilde{\mathbf{A}}(\mathbf{p})$ and $\tilde{\mathbf{E}}(\mathbf{p})$ are defined, assuming that the parameter vector is defined as $\mathbf{p} = (m, K_h)$, as follows:

$$\tilde{\mathbf{A}}(\mathbf{p}) = \mathbf{A}_0 + m\mathbf{A}_m + K_h\mathbf{A}_K, \qquad \mathbf{E}(\mathbf{p}) = \mathbf{E}_0 + m\mathbf{E}_m + K_h\mathbf{E}_K \tag{41}$$

In contract notation, it is possible to write

$$\mathbf{S}\,(\mathbf{p}) = \begin{pmatrix} \tilde{\mathbf{A}}(\mathbf{p}) + j\mathbf{E}(\mathbf{p}) & \tilde{\mathbf{B}}(\mathbf{p}) \\ \mathbf{C}(\mathbf{p}) & \mathbf{D}(\mathbf{p}) \end{pmatrix}, \qquad \mathbf{S}_i = \begin{pmatrix} \tilde{\mathbf{A}}_i + j\mathbf{E}_i & \tilde{\mathbf{B}}_i \\ \mathbf{C}_i & \mathbf{D}_i \end{pmatrix} \tag{42}$$

The system coefficients $\mathbf{S}_0, \ldots, \mathbf{S}_n$ fully characterize the dependence on the uncertain parameters $\mathbf{p} = (p_1, \ldots, p_n)$. Note that the system coefficient $\mathbf{S}_0, \ldots, \mathbf{S}_n$ does not need to represent any meaningful dynamical system, but that only their combination $\mathbf{S}(\mathbf{p})$ is a relevant description of the problem [20]. The parameter uncertainty is quantified by the range of parameter values and possibly the rates of parameter variation. The parameter uncertainty range can be

Table 1 Geometrical parameters of the wing model

Parameters and values	
$b = 1$ ft	$r = 1.0$
$x_{\text{EA}} = -0.3$	$m = 2.6883$ slugs
$K_\alpha = 0.2 \times 100^2 I_\alpha$ slugs · ft/s^2	$I_\alpha = 0.25 \times 6.04868$ slugs · ft^2/ft
$K_\beta = 0.2 \times 300^2 I_\beta$ slugs · ft/s^2	$I_\beta = 0.25 \times 0.151217$ slugs · ft^2/ft
$K_h = 0.2 \times 50^2$ m (slugs/s^2)	$S_\alpha = 0.3 \times 0.61298$ slugs
$\rho = 0.002378$ slugs/ft^3	$S_\beta = 0.3 \times 0.10081$ slugs

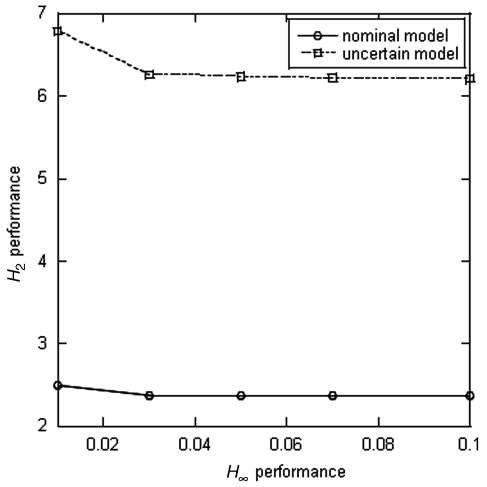

Fig. 5 H_∞ and H_2 tradeoff performance study.

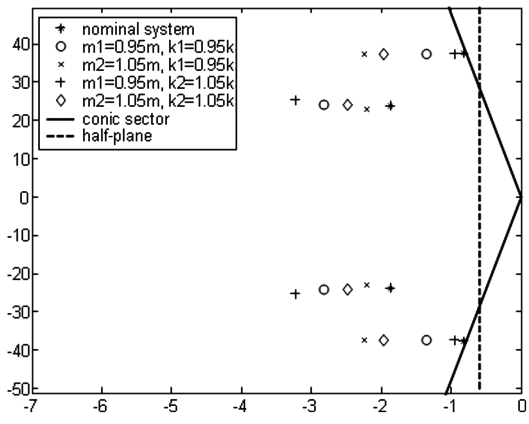

Fig. 6 Closed-loop system poles in the LMI region.

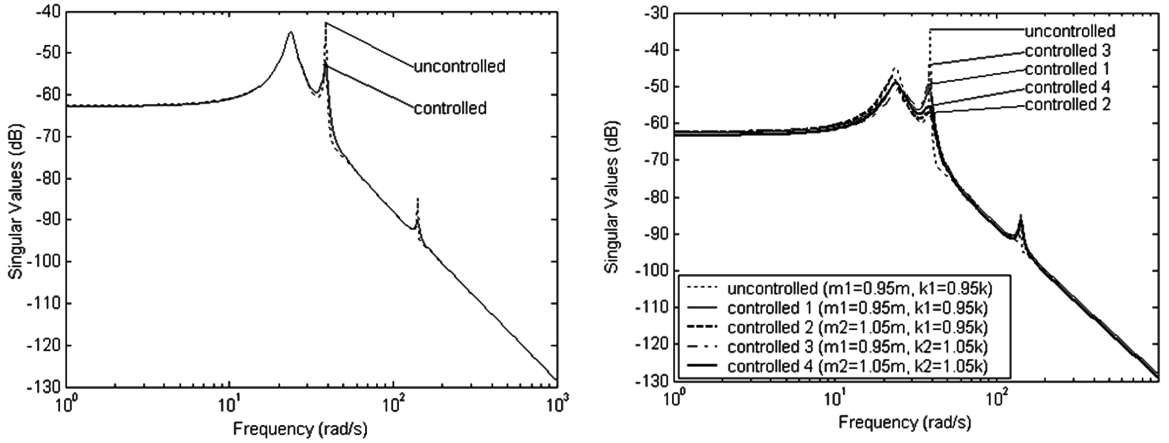

a) b)

Fig. 7 Singular value plots of the models: a) nominal, and b) uncertain.

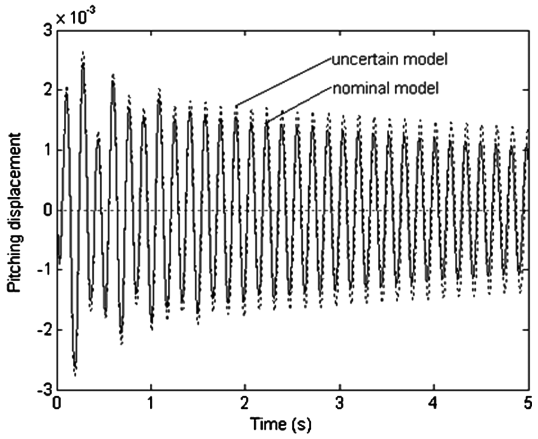

Fig. 8 Effects of parametric uncertainty on the pitching time-history impulse response.

described as a box in the parameter space. This corresponds to cases in which each uncertain or time-varying parameter p_i ranges between two empirically determined extreme values, $\underline{p}_i$ and $\bar{p}_i$:

$$p_i \in [\underline{p}_i, \bar{p}_i] \tag{43}$$

Notice that, in the proposed model, the time-varying parameter, that is, the rate of variation, have not been considered.

VI. Numerical Simulations and Discussions

The geometrical and physical characteristics of the 3-DOF airfoil to be used in the present numerical simulations are presented in Table 1. The flutter speed for this model is $V = 457$ ft/s. As remarked in [15], from a mathematical point of view, it can be assumed that, instead of moving the flap with a required deflection, an equivalent control hinge moment can be incorporated into the open-loop aeroelastic governing Eq. (5). This is analytically valid because this external moment acts on the flap hinge and affects only β DOF.

In the presence of external time-dependent excitations, the determination of the time history of the quantities $(\tilde{h}(\equiv h/b), \alpha, \beta)$, at any flight speed lower than the flutter speed, requires the solution of a boundary-value problem. Figure 5 shows a tradeoff relation between the H_∞ performance and the H_2 performance. By inspecting the curves, the state-feedback gain obtained for $\gamma = 0.03$ yields the best compromise between the mixed objectives.

Figure 6 shows that the closed-loop system poles are located in the intersection of the LMI region, a conic sector and a half-plane. By means of regional pole placement constraints, a conic sector and half-plane, closed-loop poles of the uncertain system are located in their intersection. It should be noted that the uncertainty of the present model is 5% perturbations of mass and stiffness of the system, respectively. Singular value plots of the nominal and uncertain models are presented in Fig. 7. Three peak values in both the nominal and uncertain models can be found. For a square state matrix system, the peaks' value in the frequency domain plot are indicative of the natural frequencies of the system, for example, the plunging,

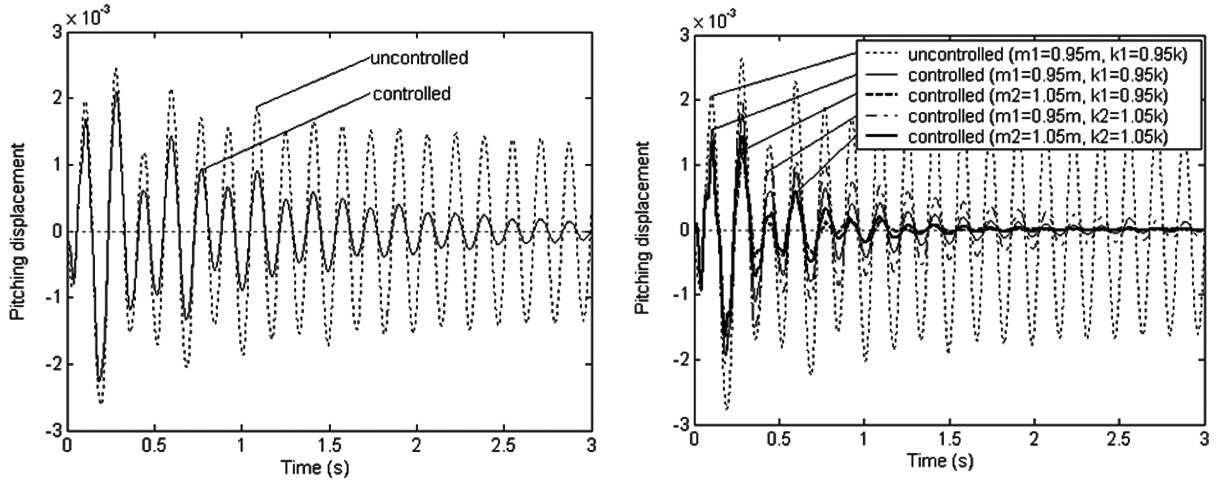

a) b)

Fig. 9 Uncontrolled/controlled pitching time-history impulse response: a) nominal, and b) uncertain.

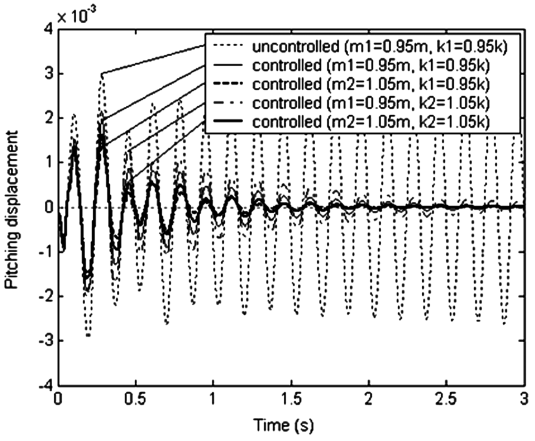

Fig. 10 Robustness to model uncertainty at flutter speed.

pitching, and flapping frequencies correspond to the peak value frequencies in the singular value plots. The largest peak value in the singular value plot refers to the H_∞ norm of the transfer matrix. In both the nominal and uncertain model case, the largest singular value is well below the one in the controlled mode. Figure 8 shows the effect of parameter uncertainty on the pitching aeroelastic response of the 3-DOF system to an impulse. In this specific case, the uncertain model has a larger amplitude than the nominal one. The robust control performances of the multi-objective synthesis of the aeroelastic system without and with uncertainties are presented in Fig. 9. In the system with uncertainties, the mass and stiffness have been modified within $\pm 5\%$ the nominal case, and the response of the uncontrolled and controlled cases have been depicted. In all four models considered, similar well-controlled responses have been achieved. This shows that the controller has quite a good performance in spite of the four bound uncertainty values with respect to model uncertainty. The simulations presented so far are at the subcritical flight speed of $V = 430$ ft/s.

In Fig. 10, the impulse response at the flutter speed of $V_F = 457$ ft/s is shown. As expected, with increasing time, the uncontrolled response diverges and become unstable with one set of the bound values. Once the controller is in operation, the amplitude decreases remarkably in a very short time. In view of the performance of the present multi-objective control scheme, the flutter speed can be increased to $V_F = 520$ ft/s.

VII. Conclusions

The high efficiency of the implemented robust control strategy applied to lifting surfaces under model uncertainty was presented. Results are related to the aeroelastic response and robust control of the 3-DOF airfoil operating in an incompressible flowfield. The multi-objective state-feedback control law using a mixed H_∞/H_2 design is robust to model uncertainty and various disturbances. However, although a 13% increase of flutter boundary was obtained with the proposed design, the implementation of the present controller may be limited by a larger control energy input required as compared with conventional control methods.

Acknowledgments

The authors would like to acknowledge Liviu Librescu of Virginia Tech, whose help, guidance, and support through the years have made this research possible. He will be remembered and deeply missed. Sungsoo Na also acknowledges the support by the Korea Science and Engineering Foundation grant funded by the Korea government (no. R11-2007-028-00000-0). Pier Marzocca would like also to acknowledge the partial funding support of National Science Foundation grant no. OISE-0532683.

References

[1] Librescu, L., and Marzocca, P., "Advances in the Linear/Nonlinear Control of Aeroelastic Structural Systems," *Acta Mechanica*, Vol. 178, Nos. 3–4, 2005, pp. 147–186. doi:10.1007/s00707-005-0222-6

[2] Mukhopadhyay, V., (ed.), "Benchmark Active Control Technology: Part I," *Journal of Guidance, Control, and Dynamics*, Vol. 23, No. 5, 2000, pp. 913–960. doi:10.2514/2.4631

[3] Mukhopadhyay, V., (ed.), "Benchmark Active Control Technology: Part II," *Journal of Guidance, Control, and Dynamics*, Vol. 23, No. 6, 2000, pp. 1093–1139. doi:10.2514/2.4659

[4] Mukhopadhyay, V., (ed.), "Benchmark Active Control Technology: Part III," *Journal of Guidance, Control, and Dynamics*, Vol. 24, No. 1, 2001, pp. 146–192. doi:10.2514/2.4693

[5] Friedmann, P. P., Guillot, D., and Presente, E., "Adaptive Control of Aeroelastic Instabilities in Transonic Flow and Its Scaling," *Journal of Guidance, Control, and Dynamics*, Vol. 20, No. 6, 1997, pp. 1190–1199. doi:10.2514/2.4175

[6] Lind, R., and Brenner, M., *Robust Aeroservoelastic Stability Analysis*, Springer–Verlag, New York, 1999.

[7] Barker, J. M., and Balas, G. J., "Comparing Linear Parameter-Varying Gain-Scheduled Control Techniques for Active Flutter Suppression," *Journal of Guidance, Control, and Dynamics*, Vol. 23, No. 5, 2000, pp. 948–955. doi:10.2514/2.4637

[8] Scott, R. C., and Pado, L. E., "Active Control of Wind-Tunnel Model Aeroelastic Response Using Neural Networks," *Journal of Guidance, Control, and Dynamics*, Vol. 2, No. 6, 2000, pp. 1100–1108.

[9] Guillot, D. M., and Friedmann, P. P., "Fundamental Aeroservoelastic Study Combining Unsteady Computational Fluid Mechanics with Adaptive Control," *Journal of Guidance, Control, and Dynamics*, Vol. 23, No. 6, 2000, pp. 1117–1126. doi:10.2514/2.4663

[10] Zhang, R., and Singh, S. N., "Adaptive Output Feedback Control of an Aeroelastic System with Unstructured Uncertainties," *Journal of Guidance, Control, and Dynamics*, Vol. 24, No. 3, 2001, pp. 502–509. doi:10.2514/2.4739

[11] Zeng, Y., and Singh, S. N., "Output Feedback Variable Structure Adaptive Control of Aeroelastic Systems," *Journal of Guidance, Control, and Dynamics*, Vol. 21, No. 6, 1998, pp. 830–837. doi:10.2514/2.4342

[12] Xing, W., and Singh, S. N., "Adaptive Output Feedback Control of a Nonlinear Aeroelastic Structure," *Journal of Guidance, Control, and Dynamics*, Vol. 23, No. 6, 2000, pp. 1109–1116. doi:10.2514/2.4662

[13] Behal, A., Rao, V. M., Marzocca, P., and Kamaludeen, M., "Adaptive Control for a Nonlinear Wing Section with Multiple Flaps," *Journal of Guidance, Control, and Dynamics*, Vol. 29, No. 3, 2006, pp. 744–748. doi:10.2514/1.18182

[14] Rao, V. M., Behal, A., Marzocca, P., and Rubillo, C., "Adaptive Aeroelastic Vibration Suppression of a Supersonic Airfoil with Flap," *Aerospace Science and Technology*, Vol. 10, No. 4, 2006, pp. 309–315. doi:10.1016/j.ast.2006.03.006

[15] Librescu, L., Na, S., Marzocca, P., Chung, C., and Kwak, M., "Active Aeroelastic Control of 2-D Wing-Flap Systems Operating in an Incompressible Flowfield and Impacted by a Blast Pulse," *Journal of Sound and Vibration*, Vol. 283, Nos. 3–5, 2005, pp. 685–706. doi:10.1016/j.jsv.2004.05.010

[16] Gahinet, P., Nemirovski, A., Laub, A. J., and Chilali, M., *LMI Control Toolbox*, The MathWorks, Inc., Natick, MA, 1995.

[17] Zhou, K., and Doyle, J. C., *Essentials of Robust Control*, Prentice–Hall, Upper Saddle River, NJ, 1998.

[18] Doyle, J., Zhou, K., Glover, K., and Bodenheimer, B., "Mixed H_2 and H_∞ Performance Objectives II: Optimal Control," *IEEE Transactions on Automatic Control*, Vol. 39, No. 8, 1994, pp. 1575–1587. doi:10.1109/9.310031

[19] Scherer, C., Gahinet, P., and Chilali, M., "Multi-Objective Output-Feedback Control via LMI Optimization," *IEEE Transactions on Automatic Control*, Vol. 42, No. 7, 1997, pp. 896–911. doi:10.1109/9.599969

[20] Ogata, K., *Modern Control Engineering*, Prentice–Hall, Englewood Cliffs, NJ, 1997.